Collective excitations, Nambu-Goldstone modes, and instability of inhomogeneous polariton condensates

Ting-Wei Chen,[1] Szu-Cheng Cheng,[2,*] and Wen-Feng Hsieh[1,3,†]
[1]*Department of Photonics, National Cheng Kung University, Tainan, Taiwan*
[2]*Department of Optoelectric Physics, Chinese Culture University, Taipei, Taiwan*
[3]*Department of Photonics and Institute of Electro-Optical Engineering, National Chiao Tung University, Hsinchu, Taiwan*
(Received 28 October 2011; revised manuscript received 15 September 2013; published 8 November 2013)

We study nonequilibrium polariton condensates in a harmonic potential trap. After finding the steady-state density and supercurrent distributions of nonequilibrium condensates, we calculate the collective excitations of the system. From collective excitation spectra, we can identify the bifurcation of the stable and unstable modes in terms of the pumping spot size and power. There exist Nambu-Goldstone modes that reveal the pattern of the spontaneous symmetry breaking of the system. Moreover, the unstable mechanism associated with the inward supercurrent flow is characterized by the existence of a supersonic region within the condensate.

DOI: 10.1103/PhysRevB.88.184502 PACS number(s): 05.30.Jp, 03.75.Kk, 47.20.Ky, 71.36.+c

I. INTRODUCTION

In the past years, there have been intensive searches for a new Bose-Einstein condensate in solids. Researchers found such a candidate called the microcavity-polariton condensate (MPC), which has been created from the interaction of cavity photons and confined excitons in the strong-coupling regime.[1,2] Growing research activities in this MPC can be attributed to the system being intrinsically out of equilibrium determined by the dynamical balance between interactions, trapping potentials, pumping and decay.[3] Rich phenomena from nonequilibrium many-body physics are accessible in this system. Many signatures of phase transition from inhomogeneous MPCs, such as spectral and spatial narrowing and first-order coherence, were studied by Balili *et al*.[4] Moreover, there exists superfluidity even though the MPC involves a nonequilibrium dissipative character.[5–7] Due to the continuous pumping and disorders of MPCs, the instability of rotationally symmetric states and vortices appear spontaneously without stirring or rotating MPCs.[7,8] Nonequilibrium MPCs also show rotational spontaneous symmetry breaking and are unstable towards the formation of vortices or vortex array without any rotational drive.[9–11] Although the spontaneous symmetry breaking followed by nonequilibrium MPCs has been experimentally demonstrated, the properties of spontaneous symmetry-breaking states still need to be understood and are worthily studied.

Nonequilibrium MPCs have been theoretically investigated by several groups, for instance, Keeling *et al*.[9,10] studied the slow dynamics of MPCs by eliminating the reservoir dynamics, while Wouters and Carusotto[12] coupled the dynamics of polaritons from condensate to the reservoir with rate-diffusion equation in homogeneous systems. Both Refs. 10 and 12 concluded the same excitation behavior of diffusive Goldstone modes at low momentum, which is recognized as a unique feature coming from the driven-dissipative systems.[13] However, Ref. 12 dealt with homogeneous MPCs, and the specification of the Thomas-Fermi (TF) radius as the unstable boundary in Ref. 9 is not always valid since the effects of the density gradient and supercurrent of the steady state cannot be neglected under the regime of higher pump powers. The excitation spectra of inhomogeneous MPCs have been observed experimentally,[14,15] and no theoretical model can characterize these spectra accurately for finite-size MPCs.

In this paper, we apply the complex Gross-Pitaevskii equation (cGPE) to model nonequilibrium MPCs in a harmonic potential trap.[9,10] In Sec. II, we calculate the steady states of MPCs. The density and supercurrent distributions are given for various pumping conditions. Once we find the steady states of MPCs. We then study the collective excitation spectra and stability of MPCs in Sec. III. The collective excitation spectra show the possible existence of Nambu-Goldstone modes that can reveal the pattern of the spontaneous symmetry breaking of MPCs. In Sec. IV, a phase boundary between the stability and instability of the system is identified. From comparing this phase boundary with the supersonic horizon, we interpret the unstable mechanism of a MPC being due to the existence of an inward and supersonic flow in the steady state. The conclusion is given in Sec. V.

II. STEADY STATES OF POLARITON CONDENSATES IN A TRAP

The cGPE is a mean-field model developed to deal with the many-body problems incorporating the trapping potential, interparticle interactions, pumping, and decay dynamics.[9,10] The trapping potential is given by a harmonic potential $V_{\text{ext}} = (\hbar\omega/2)(r^2/\lambda^2)$ with trapping frequency ω and oscillator length $\lambda = \sqrt{\hbar/m\omega}$, where $\hbar$ and m are Planck's constant and polariton mass, respectively. By choosing the length, time, and energy scales in units of λ, $1/\omega$, and $\hbar\omega$, respectively, and further rescaling the wave function $\psi \to \sqrt{\hbar\omega/2U}\psi$ with respect to the strength of the two-body interaction potential U, we obtain the dimensionless cGPE (Ref. 9)

$$i\frac{\partial}{\partial t}\psi = \left[-\frac{1}{2}\nabla^2 + \frac{r^2}{2} + \frac{1}{2}|\psi|^2 + \frac{i}{2}(\alpha - \sigma|\psi|^2)\right]\psi, \quad (1)$$

where the third term on the right-hand side of the equation represents the normalized two-body interaction, the dimensionless linear net gain $\alpha = 2\gamma/\hbar\omega$ represents the pump power with γ describing the balance between the stimulated scattering of polaritons into the condensate and the decay of polaritons out of the cavity, and $\sigma = \Gamma/U$ is a factor of the

nonlinear effective loss with Γ being the coefficient of gain saturation.

We consider the pumping profile being inhomogeneous and shown as $\alpha(r) = P[\Theta(r) - \Theta(r - R)]$, where P is the pump power, $\Theta(r - R)$ is a unit step function, and R is the pump spot size. With σ being fixed ($\sigma = 0.3$) throughout this paper, the physical properties of the system are determined by pumping parameters P and R. The steady state of a MPC is shown by the wave function $\psi(\mathbf{r},t) = \psi_0(\mathbf{r})e^{-i\mu t}$, where μ is the chemical potential of the system for given pumping parameters P and R, and is determined by the conservation law of polaritons

$$\int (\alpha - \sigma|\psi|^2)|\psi|^2 d^2r = 0, \tag{2}$$

i.e., the balance between net gain and loss over all the space being zero.

From the Madelung transformation, we take $\psi_0(\mathbf{r}) = \sqrt{\rho(\mathbf{r})}e^{i\phi(\mathbf{r})}$, where $\rho(\mathbf{r})$ and $\phi(\mathbf{r})$ are the density and phase of a MPC, respectively. Given the supercurrent $\mathbf{v}(\mathbf{r}) = \nabla\phi$ and from Eq. (1), we can obtain the continuity and Bernoulli's equations:

$$\nabla \bullet (\rho\mathbf{v}) = (\alpha(r) - \sigma\rho)\rho, \tag{3}$$

$$\frac{1}{2}(r^2 + \rho) + \frac{1}{2}|\mathbf{v}|^2 - \frac{1}{2\sqrt{\rho}}\nabla^2(\sqrt{\rho}) = \mu. \tag{4}$$

If the pump power is uniformly distributed, the quantum pressure, $\nabla^2(\sqrt{\rho(r)})/\sqrt{\rho(r)}$, and the supercurrent have a small effect on the density distribution. From Eq. (4), we then find the TF solution of the system with the rotationally symmetric density and supercurrent being $\rho(r) = a^2 - r^2$ and $v(r) = -Pr(a^2 - r^2)/4a^2$, respectively, where the TF radius $a = \sqrt{3P/2\sigma}$ is determined by the balance of net gain and loss of Eq. (3). Due to the possible existence of a supersonic horizon, we shall compare the supercurrent with the sound velocity c of a MPC and define a velocity-comparison factor $f = 1 - (v/c)^2$, where the sound velocity $c = \sqrt{\rho(r)/2}$ is obtained by varying the pressure of the barotropic equation of state with respect to the mass density of the condensate fluid.[18] The supercurrent profiles exhibit certain subsonic or supersonic regions shown by the factor f being greater or less than zero, respectively. The velocity-comparison factor of the TF solution is $f(r) = 1 - [(Pr)^2(a^2 - r^2)/8a^4]$. Note that the TF solution does not describe the system correctly. It just gives us a crude physical picture of the MPCs.

To find the accurate steady state of the MPCs, we solve Eqs. (3) and (4) numerically by applying the shooting method[16,17] with the fourth-order Runge-Kutta integration under the constraint of Eq. (2). The rotationally symmetric distributions of the steady-state densities $\rho(r)$, supercurrents $v(r)$, and velocity-comparison factors $f(r)$ of MPCs are shown in Fig. 1 for $R = 2$ (green dotted lines), $R = 4$ (red-dash dotted lines) and $R = 8$ (blue solid lines) under $P = 4.4$. Note that the variation of the pump power is equivalent to the effect of changing the pumping spot size. When we decrease/increase the pump power, the MPC cloud shrinks or grows and the pumping spot size becomes larger or smaller than the MPC size due to shortage or abundance of net gain on the edge of the MPC, respectively. In addition, due to repulsive interactions

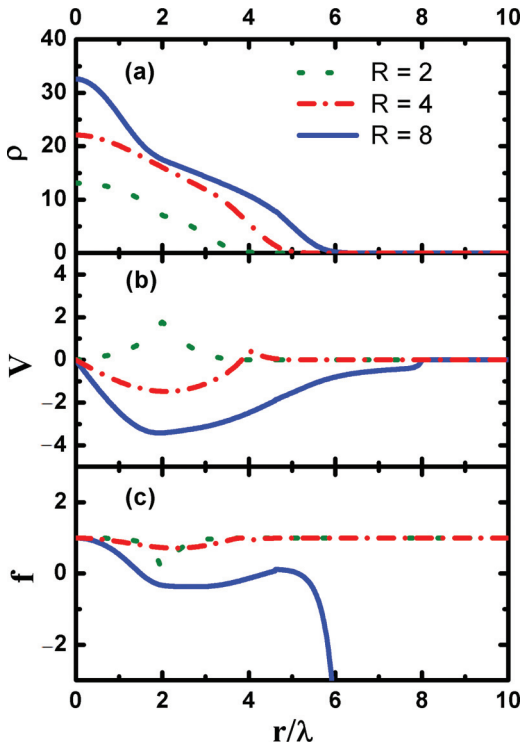

FIG. 1. (Color online) Stationary solutions of the condensate. (a) Density distributions, (b) supercurrent distributions, and (c) velocity comparison factors for the pumping power $P = 4.4$ and pumping spot sizes $R = 8$ (blue solid lines), $R = 4$ (red dash dotted lines), and $R = 2$ (green dotted lines), respectively.

of polaritons, the chemical potential of the condensate raises and creates a blueshift on the total energy because more polaritons have been injected into the system by raising the pump power.[14]

The size and density of the MPC increase with increasing pumping radius R, as in Fig. 1(a), that is consistent with the previous results.[9] Note that the supercurrent distribution not shown in Ref. 9 but obtained by the series expansion, which is valid only for near the center of the MPC, was shown in the appendix of Ref. 10. So far to the best of our knowledge, there is no full-range supercurrent distribution being calculated. Here, we have determined the steady state of MPC by not only the density distribution but also the supercurrent distribution. The density profiles of MPCs are quite different from the TF density profiles due to nonzero supercurrents, resulting from the nonequilibrium pump and decay characters of MPCs. The density distribution of the system is affected by the supercurrent: the higher or lower density at any position corresponding to a smaller or larger supercurrent.[9] For $R = 8$, the density is suppressed near $r = 2$, where the magnitude of the supercurrent is maximal.

Shown in Fig. 1(b), the supercurrent of the nonequilibrium flow of MPC depends on the pumping spot size and power. This flow is given by the continuity equation of Eq. (3), in which the gain of the MPC is density dependent. If the density is low, then the gain dominates; however, if the density is high, then the density-dependent and dissipative term dominates,

and the condensates in the high-density region flow toward the low-density region. Consequently, the supercurrents must exist in between the high- and low-density regions. The supercurrent of a flow is lower or higher with respect to the higher or lower density at any position. This correlation between the density and supercurrent can be understood from Eq. (4). When the pump power is not very high, we can neglect the quantum pressure in Eq. (4). Supercurrents are zero outside the MPC and at the center of the trap. There exist a maximal supercurrent somewhere in the middle region of the MPC, where the density has to be lowered in order to preserve the chemical potential. Thus, the radial position of the maximal supercurrent corresponds to the position of density depletion. Indeed, as shown in Fig. 1(b) of the steady-state solutions of MPCs, we find that there is a maximal supercurrent happening at the density suppression that increases with increasing R.

Because the supercurrent increases with increasing R, as the pumping spot size is increased above some critical value R_c, there is a supersonic region, where the supercurrent is higher than the sound velocity and the velocity-comparison factor $f < 0$. From Fig. 1(c) the velocity-comparison factor f becomes negative in the region of $r > 1.5$ for the supercurrent profile of the MPC with $R = 8$. If the supersonic phenomenon happens within the MPC, we shall see that a small perturbed MPC generates rotationally symmetric-breaking states, rotons, and vortices, and the MPC becomes unstable. Moreover, in such a system of MPCs in a potential trap, the steady-state flow, which exceeds the speed of sound, can be achieved. Within the corresponding event horizons, the sound waves (sonic perturbations) that cannot escape from the event horizons instead are dragged inwards. If the condensate supercurrent is slow, the excitations propagate with the sound velocity, whereas if the condensate supercurrent is faster than the sound velocity, then the excitations cannot propagate against the background stationary flow, and, in theory, the information cannot be transported. It is the supersonic flow that contributes to the instabilities rather than the inward superfluid flow concluded in Refs. 9 and 10. For the MPC with $R = 4$ shown in Fig. 1(b), the radial supercurrent is an inward flow, but it is stable and will be shown later. We also observed the flow direction of the supercurrent, depending on the pumping spot size: the outward and inward flows correspond to the smaller and larger pumping spot sizes, respectively. In a trap, a small perturbation on the MPC can change its original flow along the radial direction into the azimuthal direction spontaneously. The system then becomes spontaneously rotational symmetry breaking and contains many degenerate states labeled by the quantum number ℓ of angular momentum. According to Goldstone's theorem, excitation modes of a spontaneous symmetry-breaking system will have gapless modes, called the Nambu-Goldstone modes.[18] The Nambu-Goldstone modes are the dominant excitation modes at small wave vector (or in the long wavelength limit) of excitations of the system.[19] Therefore, it is fruitful that we can find the excitation mode pattern of MPCs in order to understand the phenomena of spontaneously rotational symmetry breaking occurring in MPCs. In the following, we calculate the collective excitation spectra of MPCs in a trap by using a perturbation method.[20]

III. COLLECTIVE EXCITATION SPECTRA AND STABILITY OF POLARITON CONDENSATES IN A TRAP

We investigate the spontaneous symmetry-breaking properties of MPCs from the Nambu-Goldstone modes that occur in the collective excitation spectrum and study the stability of MPCs. In order to study the dynamical properties of MPCs with respect to pumping schemes (conditions of varying the pumping spot size and power), we apply a small perturbation $\delta\psi(\mathbf{r},t) = e^{-i\mu t}[u(\mathbf{r})e^{-i\Omega t} - w^*(\mathbf{r})e^{i\Omega t}]$ on the steady state $\psi_0(\mathbf{r})$, where Ω is the excitation frequency of the system. Substituting the total wave function $\psi(\mathbf{r},t) = \psi_0(\mathbf{r}) + \delta\psi(\mathbf{r},t)$ into Eq. (1) and linearizing it around the steady state $\psi_0(\mathbf{r})$, we obtain a pair of Bogoliubov's equations[21] for excitations. Because of the rotational invariance of the condensate, $u(\mathbf{r})$ and $w(\mathbf{r})$ of Bogoliubov's equations can be written as: $u(\mathbf{r}) = U(r)e^{i\phi(r)}e^{\pm i\ell\theta}$ and $w(\mathbf{r}) = W(r)e^{-i\phi(r)}e^{\pm i\ell\theta}$, where ℓ and θ are the quantum numbers of angular momentum and the azimuthal angle, respectively. We then obtain the Bogoliubov equations:

$$L[U] - \tfrac{1}{2}(\rho - i\sigma\rho)W = (\mu + \Omega)U, \tag{5}$$

$$L^\dagger[W] - \tfrac{1}{2}(\rho + i\sigma\rho)U = (\mu - \Omega)W, \tag{6}$$

where

$$L = -\frac{1}{2}e^{-i\phi}\frac{1}{r}\frac{d}{dr}\left(r\frac{d}{dr}e^{i\phi}\right) + \left[\frac{\ell^2}{2r^2} + \frac{r^2}{2} + \rho + \frac{i}{2}\alpha - i\sigma\rho\right] \tag{7}$$

and $L^\dagger$ is the adjoint operator of L. From solving eigenfunctions and eigenfrequencies of Eqs. (5) and (6) under different pumping schemes, we find the collective excitation states and their excitation energies of the condensate as a function of ℓ.

Because of the nonequilibrium character of MPCs, Eqs. (5) and (6) are non-Hermitian, and excitation frequencies Ω are complex values,[12,13] whose real part, $\mathrm{Re}(\Omega)$, and imaginary part, $\mathrm{Im}(\Omega)$, display the excitation energy and decay (or growth) rate of the condensate, respectively. The decay, $\mathrm{Im}(\Omega) < 0$, or growth, $\mathrm{Im}(\Omega) > 0$, behavior of collective excitation modes indicates the steady state of the condensate is stable or unstable, respectively. The dispersion curves of low-lying excitation modes of the condensate are shown in Fig. 2. These mode dispersions are quite different for various pumping conditions. As shown in Figs. 2(a)–2(c), for $R = 2$ with $P = 3$ and $R = 2$ and 4 with $P = 4.4$, the excitation modes of MPCs have $\mathrm{Im}(\Omega) < 0$ for all ℓ when the pumping spot R is smaller than the TF radius, having $a = 3.87$ (4.69) for pumping power $P = 3$ (4.4). The perturbed MPCs with $R \leqq a$ are stable and damped. The stable excitation modes basically exhibit a trend that the excitation states with the higher ℓ have more nodes and higher energies than those with the lower ℓ. The lower ℓ modes possess an energy gap and linear or long wavelength diffusive dispersions for spin modes shown in spinor polariton condensates.[10] For condensates with lower P and smaller R, the excitation energies of modes with lower ℓ are nonzero with a gap as shown in Fig. 2(a). These modes, whose decay rates are small, show underdamped rotation. If P is increased, the decay rates of these modes start to increase,

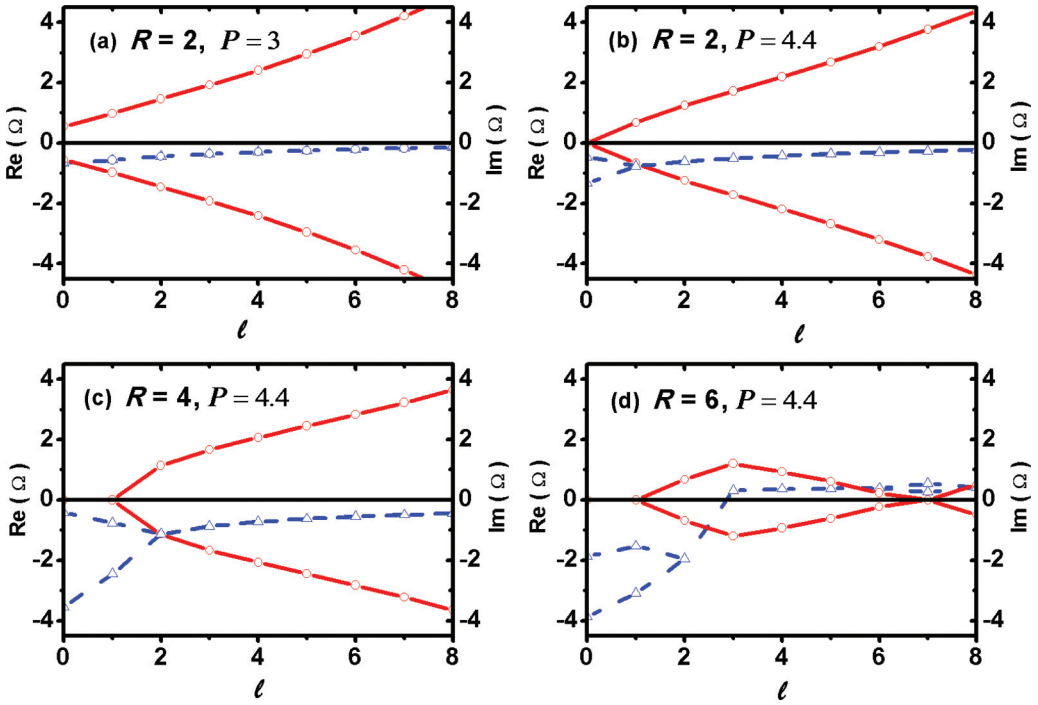

FIG. 2. (Color online) Collective excitation spectra versus quantum numbers ℓ of angular momentum. Excitation modes of (a) $R=2$, $P=3$, (b) $R=2$, $P=4.4$, (c) $R=4$, $P=4.4$, and (d) $R=6$, $P=4.4$, respectively. Red circles and blue triangles show real (left axis) and imaginary (right axis) parts of excitation spectra. Connected lines are used to visualize the trend of excitation spectra.

and their excitation energies become gapless with $\mathrm{Re}[\Omega]=0$, occurring in the excitation spectra as R becomes larger. In Fig. 2(b), those modes with the linear dispersion relation are gapless modes, which start showing a bifurcation of small decay rate at $\ell=0$ and exhibit critically damped rotation. There are gapless excitation modes at $\ell=0$ and 1 in Fig. 2(c). They are diffusive and show overdamped rotation due to high decay rates. The gapless mode at $\ell=1$ is a Nambu-Goldstone mode, whose steady-state wave function contains a node, and in this case the rotational symmetry of the condensate breaks down spontaneously. The system also tries to restore the continuous rotational symmetry of the condensate according to the Goldstone theorem. Due to the combined effect of radial and rotational currents, the steady state with nodes can spontaneously create spiral vortices observed in the previous simulations.[9] We believe that the occurrence of spontaneous vortices in MPCs is a manifestation of the spontaneously rotational symmetry breaking of MPCs. However, the Landau instability[22,23] and Feynman theory of superfluidity[24] break down for the two-dimensional (2D) confined polariton system because the $\ell=1$ vortex is still possible to be observed in the stable regime, as shown in Fig. 2(c).[25]

If R is sufficiently larger than the TF radius, the excitation modes with the higher angular momenta have the higher-density distributions in the outskirt of the condensate, and these modes become unstable dynamically due to a net gain occurring in this region, where $\mathrm{Im}(\Omega)>0$. As shown in Fig. 2(d), the value of $\mathrm{Im}(\Omega)$ changes from negative to positive at $\ell=3$. The excitation spectra exhibit gapless modes not only at $\ell=0$ and 1 but also at a higher angular momentum of $\ell=7$. We find that the condensate contains nodes and its symmetry is spontaneously broken from these gapless Nambu-Goldstone modes. The condensate with $\ell=1$, whose $\mathrm{Im}(\Omega)<0$, generates a stable vortex with a single-flux quantum. The condensate with $\ell=7$, whose $\mathrm{Im}(\Omega)>0$, generates an unstable vortex with a multiflux quantum, and this vortex will break into stable arrays of vortices with a single-flux quantum due to the repulsive effect between fluxes. The existence of Nambu-Goldstone modes with higher ℓ in the condensate confirm and explain the mechanism of instability forming spontaneous vortex lattices seen by Keeling and Berloff, if R is larger than the TF radius.[9]

IV. PHASE DIAGRAM OF POLARITON CONDENSATES IN A TRAP

In order to understand the mechanism of stable and unstable excitation modes, the density and velocity distributions of excitation modes for $R=6$ and $P=4.4$ in Fig. 2(d) are compared. As shown in Fig. 3(a), we find that the flow velocities of excitation mode at $\ell=2$ are not considerable, so the perturbation of this mode on the condensate will hardly propagate, and the system is stable ($\mathrm{Im}(\Omega)<0$). By contrast, the excitation mode at $\ell=3$ flows inward with large velocity. The fluctuation of this mode on the condensate propagates fast and is enhanced to create the instability of the steady state ($\mathrm{Im}(\Omega)>0$), as shown in Figs. 3(b) and 3(c). For the dynamically unstable modes, the angular excitations of u and w originated in the edge are not only of the same flow direction but also large enough to reinforce the growth of the excitations and to propagate toward the center of the condensate, resulting in the instability of the steady state. Therefore, we conclude that the onset of instability is related to the simultaneous inwards flows of excited quasiparticles with higher angular momenta.

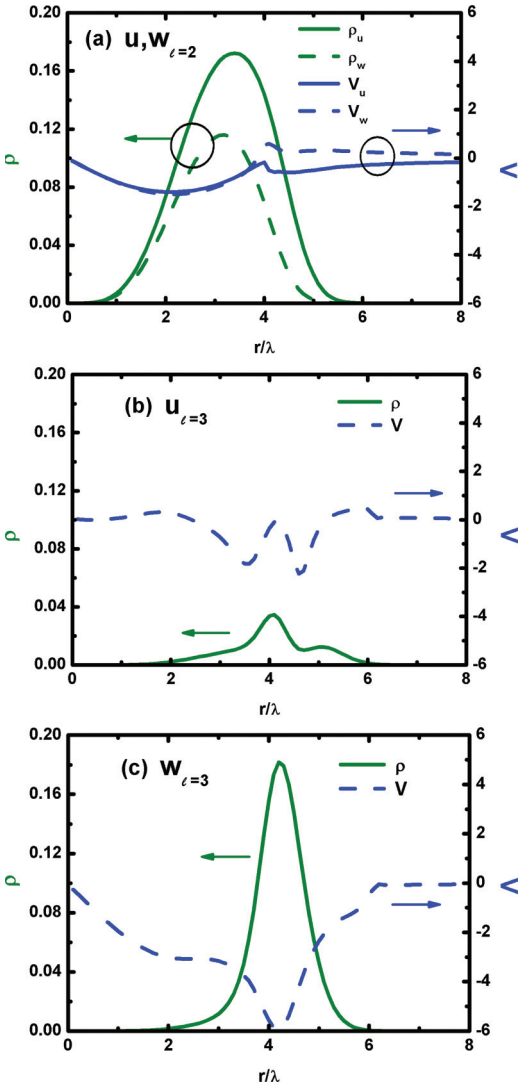

FIG. 3. (Color online) The density and flow velocity of excited quasiparticles u and w calculated from Fig. 2(d). (a) Angular momentum $\ell = 2$, (b) angular momentum $\ell = 3$ for u, and (c) angular momentum $\ell = 2$ for w.

To further discuss the instability of MPCs, we plot the phase diagram of stability of steady states in Fig. 4 in terms of P and R. It shows the phase boundary with relevant pumping schemes at which the phase transition takes place (see empty circles in Fig. 4). MPCs in a trap are stable or unstable as P goes higher or lower and R is smaller or bigger. Note that the boundary between the stable and unstable states basically follows a line through the turning points of the constant chemical potential curves.[26] By analogy to the definition of the isothermal compressibility, $\beta_T = -\frac{1}{V}(\frac{\partial V}{\partial P})_T$, which measures the relative volume (V) change of matter by the applied pressure (P) at constant temperature (T), we define an isopotential compressibility as $\beta_\mu = -\frac{1}{R}(\frac{\partial R}{\partial \alpha})_\mu$, which measures the relative change of pump spot (R) by the applied pump strength P/P_{th} (proportional to the strength parameter α) at constant chemical potential (μ) in our system. Therefore, negative isopotential compressibility defines the stability of the condensate, and the condensate behaves with positive compressibility when crossing from the stable to unstable region.

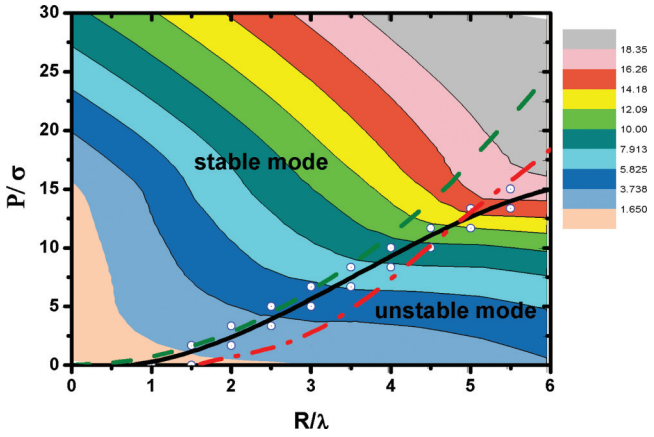

FIG. 4. (Color online) Phase diagram of the condensate for various pumping spot sizes and powers with a contour of chemical potential. The dashed green line is the phase boundary from the TF approximation, and the solid black line is the numerical boundary of the stable and unstable modes. The red dash dotted line is the boundary for the subsonic and supersonic transition.

A supersonic boundary is also plotted with the intersection of the unstable boundary near the pump spot $R \sim 5$. For smaller pump strength, it is shown that, prior to the instability transition with increasing pumping spot size, the supercurrent flow velocity is slower than the sound velocity for any radial position, namely, all the regions are of subsonic flows. Conversely, for larger pump strength, the instability transition lags behind the supersonic transition that implies the initiation of supersonic flow acts as a precursor to drive the stable mode into the instability. Although the phase boundary of the TF approximation shows the same trend at low pumping strength, it does not match with the numerical boundary at high pumping power because the supercurrent of the condensate will affect the density distribution of the steady state significantly, and the density gradient in the cGPE is actually not negligible as in the TF approximation. The phase boundary determined by the TF approximation is valid only when P and R are low and small, respectively. As P and R become larger, it is invalid to use the TF radius as the criterion of forming vortex lattices simultaneously.[9]

V. CONCLUSION

In conclusion, we obtained, for the first time, the steady-state density and supercurrent profiles of inhomogeneous MPCs. Moreover, the excitation spectrum for each pumping scheme is obtained for the confined 2D system. In a trap, a small perturbation on the solutions with inward flows will cause the spontaneous symmetry breaking and show the existence of Nambu-Goldstone modes within collective excitation modes. Collective excitations also exhibit a bifurcation of stable and dynamically unstable modes with respective to the pumping spot size and power that is associated with a sign change of fluid compressibility. The onset of instability is found related to the excitation modes with inward flow and higher angular momentum ℓ, and the mechanism of dynamical instability is due to a supersonic flow within the condensate rather than the inward flow of the condensate itself.

In particular, a singly quantized vortex ($\ell = 1$) can be stable at high pumping strength, while the spontaneous vortex array can be generated from the unstable Nambu-Goldstone modes with higher angular momenta. Our observations in this paper are crucial for studying the dynamics of polariton condensates in the future. The same approach may pace a way to study the stationary states and excitations of the nonequilibrium systems, for example, the sonic black hole and chaotic systems.

ACKNOWLEDGMENTS

We acknowledge the financial support from the National Science Council (NSC) of the Republic of China under Contracts No. NSC102-2112-M-034-001-MY3 and No. NSC102-2112-M-009-016-MY3. S.C. acknowledges the support of the National Center for Theoretical Sciences of Taiwan while visiting the center.

*sccheng@faculty.pccu.edu.tw
†wfshieh@mail.nctu.edu.tw

[1] H. Deng *et al.*, Science **298**, 199 (2002).
[2] J. Kasprzak *et al.*, Nature (London) **443**, 409 (2006).
[3] H. Deng, H. Haug, and Y. Yamamoto, Rev. Mod. Phys. **82**, 1489 (2010).
[4] R. Balili *et al.*, Science **316**, 1007 (2007).
[5] M. Wouters and V. Savona, Phys. Rev. B **81**, 054508 (2010).
[6] A. Amo *et al.*, Nature (London) **457**, 291 (2009).
[7] D. Sanvitto *et al.*, Nat. Phys. **6**, 527 (2010).
[8] K. G. Lagoudakis *et al.*, Nat. Phys. **4**, 706 (2008).
[9] J. Keeling and N. G. Berloff, Phys. Rev. Lett. **100**, 250401 (2008).
[10] M. O. Borgh, J. Keeling, and N. G. Berloff, Phys. Rev. B **81**, 235302 (2010).
[11] F. M. Marchetti, M. H. Szymańska, C. Tejedor, and D. M. Whittaker, Phys. Rev. Lett. **105**, 063902 (2010).
[12] M. Wouters and I. Carusotto, Phys. Rev. Lett. **99**, 140402 (2007).
[13] M. H. Szymanska, J. Keeling, and P. B. Littlewood, Phys. Rev. Lett. **96**, 230602 (2006).
[14] S. Utsunomiya *et al.*, Nat. Phys. **4**, 701 (2008).
[15] Marc Aßmann *et al.*, Proc. Natl. Acad. Sci. USA **108**, 1804 (2011).
[16] M. A. Porras, A. Parola, D. Faccio, A. Dubietis, and P. DiTripani, Phys. Rev. Lett. **93**, 153902 (2004).
[17] A. Alexandrescu and V. M. Pérez-García, Phys. Rev. A **73**, 053610 (2006).
[18] C. Barceló, S. Liberati, and M. Visser Class, Quantum Gravity **18**, 1137 (2001).
[19] A. M. J. Schakel, *Boulevard of Broken Symmetries: Effective Field Theories of Condensed Matter* (World Scientific Publishing, Singapore, 2008).
[20] C. J. Pethick and H. Smith, *Bose-Einstein Condensation in Dilute Gases* (Cambridge University Press, New York, 2002).
[21] N. N. Bogoliubov, J. Phys. (Moscow) **11**, 23 (1947).
[22] L. D. Landau, J. Phys. (Moscow) **5**, 71 (1940).
[23] L. D. Landau, J. Phys. (Moscow) **11**, 91 (1947).
[24] R. P. Feynman, in *Progress in Low Temperature Physics*, edited by C. J. Gorter (North-Holland, Amsterdam, 1955), Vol. 1.
[25] J. Keeling and N. G. Berloff, Nature (London) **457**, 273 (2009).
[26] T. W. Chen, M. D. Wei, S. C. Cheng, and W. F. Hsieh, arXiv:1309.3012.